Chapter 7

Rupture complexity of the Great 1994 Bolivia and 2013 Sea of Okhotsk deep earthquakes

7.1 Abstract

The physical mechanism of deep earthquakes (depth>300km) remains enigmatic (Green and Houston, 1995; Houston, 2007; Kirby et al., 1996), partly because their rupture dimensions are difficult to estimate due to their low aftershock productivity (Frohlich, 1989) and absence of geodetic or surface rupture observations. The two largest deep earthquakes, the recent Great 2013 Sea of Okhotsk earthquake (M8.3) and the Great 1994 Bolivia earthquake (M8.3) (Kanamori et al., 1998; Kikuchi and Kanamori, 1994), together provide a unique opportunity to compare their rupture patterns in detail. Here we extend a travel-time sub-event location method (Duputel et al., 2012; Kikuchi and Kanamori, 1991; Tsai et al., 2005) to perform full teleseismic P-waveform inversion. This new method allows us to explain the observed broadband records with a set of sub-events whose model parameters are robustly constrained without smoothing. We find that while the Okhotsk event is mostly unilateral, rupturing 90km along strike with a velocity over 4km/s, the Bolivia earthquake ruptured about half this distance at a slow velocity (about 1.5 km/s) and displayed

a major change in rupture direction. We explain the observed differences between the two earthquakes as resulting from two fundamentally different faulting mechanisms in slabs with different thermal states. Phase transformational faulting (Green II and Burnley, 1989; Kirby et al., 1991) is inferred to occur inside the metastable olivine wedge within cold slab cores whereas shear melting (Griggs and Baker, 1969; Kanamori et al., 1998; Karato et al., 2001; Ogawa, 1987) occurs inside warm slabs once triggered.

7.2 Introduction

Several mechanisms for deep earthquakes have been proposed, including thermal shear instability (Griggs and Baker, 1969; Kanamori et al., 1998; Karato et al., 2001; Ogawa, 1987), dehydration embrittlement of pre-existing faults (Meade and Jeanloz, 1991; Silver et al., 1995), and transformational faulting associated with a metastable olivine wedge in cold subducting slabs (Green and Houston, 1995; Green II and Burnley, 1989; Kirby et al., 1991; Kirby et al., 1996). These mechanisms have been previously evaluated using deep earthquake rupture properties (e.g., duration, rupture dimension, rupture speed, stress drop, and radiation efficiency) (Suzuki and Yagi, 2011; Tibi et al., 2003; Wiens, 2001), aftershock statistics (Houston, 2007; Wiens, 2001), and their depth dependence (Persh and Houston, 2004a, b; Tocheport et al., 2007). Among these mechanisms, phase transformational faulting and thermal shear instability, possibly involving melting, have so far garnered the most evidence (Houston, 2007; Wiens, 2001). It has also been suggested that deep earthquake mechanisms may depend on the thermal state of the subducting slab (Houston, 2007; Tibi et al., 2003; Wiens, 2001; Wiens and Gilbert, 1996; Wiens and McGuire, 1995), but evidence has been inconclusive (Suzuki and Yagi, 2011).

The 1994 Bolivia earthquake was the largest deep earthquake until the recent

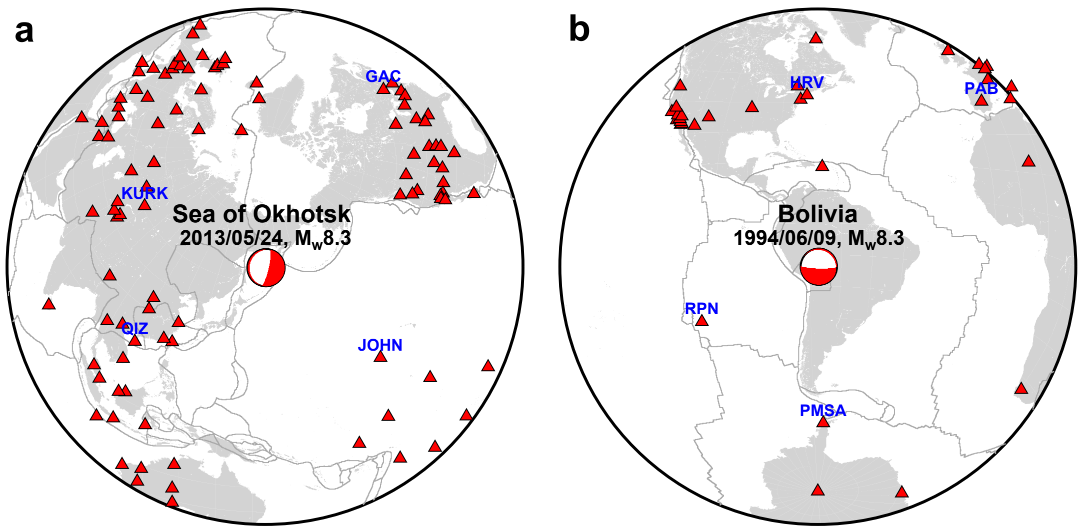

Figure 7.1: Teleseismic stations used to study (a) the 2013/05/24 Mw 8.3 Okhotsk earthquake, and (b) the 1994/06/09 Mw 8.3 Bolivia earthquake.

2013 Okhotsk earthquake of similar magnitude (Figure 7.1), and has provided critical information about deep earthquake mechanisms. The earthquake was previously characterized by low rupture speed (~1.5km/s), high static stress drop, and low radiation efficiency (Ihmlé, 1998; Kikuchi and Kanamori, 1994; Silver et al., 1995). The earthquake's rupture dimension (~30kmx40km) is small for its size, yet significantly larger than the predicted width of the metastable olivine wedge (Tibi et al., 2003), unless significant thickening of the slab occurs due to plate bending (Kirby et al., 1995). Kanamori et al. suggest instead that shear melting could have promoted extensive sliding with high energy dissipation which resulted in large slip, high stress drop and slow rupture speed (Kanamori et al., 1998).

The 2013 Okhotsk deep earthquake was of similar size as the Bolivia earthquake, but occurred in a different tectonic setting. The subducted Pacific plate in which the Okhotsk earthquake occurred is significantly older and hence colder than the subducted Nazca plate in which the Bolivia earthquake occurred (Wiens and Gilbert, 1996). A thorough comparison of these two earthquakes' rupture properties thus provides important constraints on the faulting mechanism of deep earthquakes and its temperature dependence.

7.3 Directivity analysis

Earthquake source dimension and rupture directivity directly affect the azimuth and distance dependence of waveforms. This directivity effect is easily quantified for an earthquake that consists of a few sub-events. For the n-th sub-event at time T_n with distance L_n from the hypocenter, the timing of the observed displacement pulse at any station i can be written as

$$T_n^i = T_n - \frac{L_n}{c_P^i}\cos(\theta_i - \theta_r^n),$$

where θ_i is the station azimuth, θ_r^n is the rupture direction, andc_P^i is the phase velocity of teleseismic P waves (which depends on station distance). Defining a directivity parameter following Ammon et al. (2005), $x_i = -\frac{\cos(\theta_i - \theta_r^n)}{c_P^i}$, then $T_n^i = T_n + L_n \cdot x_i$. Therefore, arranging teleseismic P waves by directivity parameter $x_i(\theta_r^n)$, different sub-events can be identified as different straight lines with slopes of L_n and zero-crossing points at T_n. The choice of rupture direction θ_r^n is based on trial and error, and could be different for different sub-events.

Figure 7.1 shows the teleseismic stations that we use for analysis of the 1994 Bolivia earthquake and the 2013 Okhotsk earthquake. We choose stations based on data quality and azimuthal coverage, and remove near-nodal stations to avoid complicated waveforms due to 3D structure. The qualitative rupture properties of a seismic event can be inferred by making the directivity plots (Silver et al., 1995). As mentioned above, arrivals from different earthquake sub-events will be aligned with different linear moveouts if the sub-events occur in the assumed rupture direction. Teleseismic

P waveforms for the Okhotsk earthquake (Figure 7.2a) show strong directivity to the NNW and SSE (N165°E), with a few major sub-events clearly visible in the directivity plot. Unlike for the Okhotsk earthquake, waveforms of the Bolivia earthquake cannot be aligned well with a single rupture direction, and require two rupture stages (Figure 7.2b, c). In stage 1, the Bolivia earthquake ruptured to the east with a series of small sub-events, whereas in stage 2 the rupture grew rapidly and the last sub-event arrival is better fit with rupture to the NE.

7.4 Subevent modeling

While the essential features of both the Okhotsk and Bolivia earthquakes are easily visualized in the directivity plots of Figure 7.2, quantitative details regarding the precise locations and timings of the sub-events cannot be determined from visual inspection. We therefore introduce a new sub-event algorithm to simultaneously invert broadband P waveforms for multiple sub-events' centroid locations, centroid times and moments. As with other sub-event methods (Duputel et al., 2012; Kikuchi and Kanamori, 1991; Tsai et al., 2005), we use only a small number of sub-events with a correspondingly small number of free parameters; yet our method can explain the observed broadband data with sufficient detail and estimate the moment distribution. Due to the small number of parameters estimated, our sub-event inversion does not require damping, smoothing or constraints on rupture velocity. Our method also uses global broadband data, rather than the regional high-frequency data of back-projection methods (Ishii et al., 2005), and therefore resolves the broadband slip distribution.

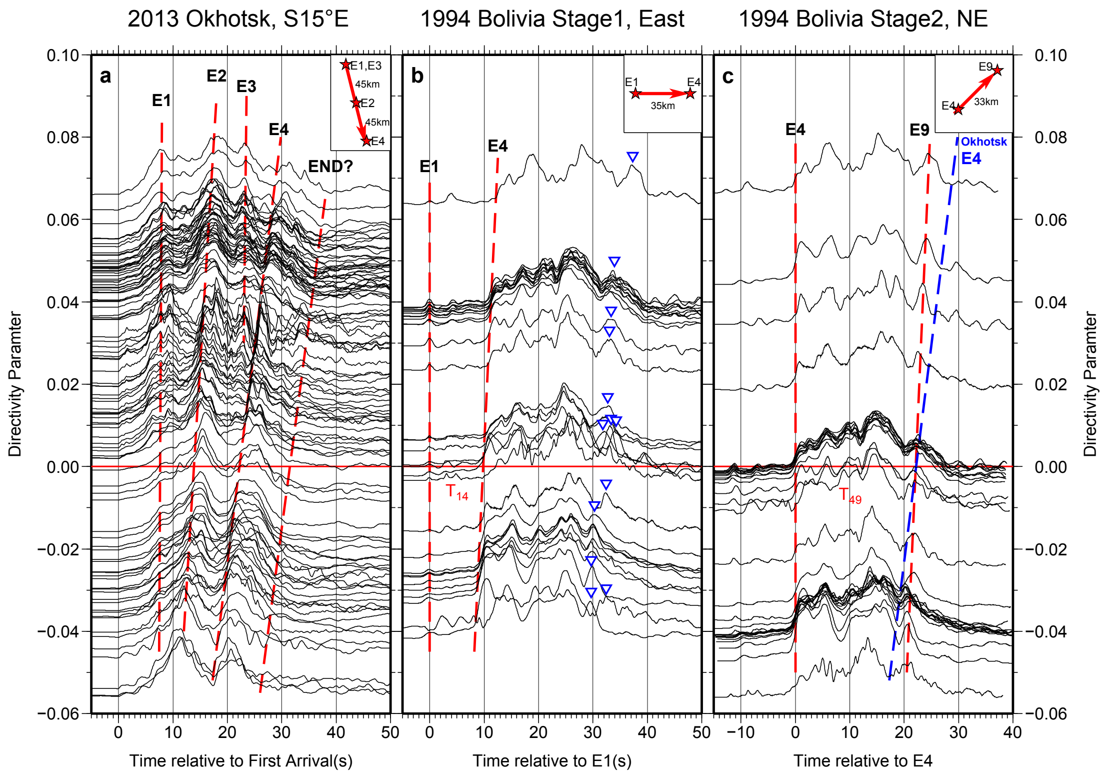

Figure 7.2: Rupture Directivity. Directivity plots for the broadband teleseismic P waves from the Okhotsk and Bolivia earthquakes. Since we do not invert for focal mechanisms here, we flip the P-wave polarities to be positive only, while keeping the true amplitudes. (a) Teleseismic P waves from the Okhotsk earthquake arranged by directivity parameter, assuming rupture direction towards S15°E and aligned by hand-picked first arrivals. We identify four major sub-events (E1, E2, E3 and E4) and the approximate end (END) marked by the red dashed lines, whose slopes are controlled by their distances from the epicenter. The times of the dashed lines at directivity parameter 0.00 identify the times of the sub-events from the earthquake origin time. The inset shows the approximate relative locations of E1, E2, E3 and E4. (b) Similar to (a) but for the Bolivia earthquake stage 1, assuming rupture direction to the East. Due to the non-emergent first arrivals, the waveforms are aligned by the first sub-event E1. Sub-event E4 denotes the sharp rise of P wave amplitudes, is well aligned, and its time from E1 is denoted as T14. The blue inverted triangles show that arrivals from the last major sub-event E9 are not well aligned by directivity to the east. (c) Similar to (b) but for the Bolivia earthquake stage 2, assuming rupture to the North-East. The P waveforms are aligned by sub-event E4. The last major sub-event E9 is delayed by T49 relative to E4, and is marked by a red dashed line. For comparison, the Okhotsk sub-event E4 from panel (a) is shown as a blue dashed line. The similar timing but steeper slope of the Bolivia E9 compared to the Okhotsk E4 suggests that the Bolivia earthquake has smaller rupture dimension and lower average speed than the Okhotsk earthquake.

7.4.1 Methods

This new algorithm is based on previous travel-time sub-event modeling (Duputel et al., 2012; Kikuchi and Kanamori, 1991; Tsai et al., 2005), but does not require the subjective hand picking of coherent arrivals. Given a set of sub-event locations and times, we first predict the sub-event arrival times for each station. We then assume Gaussian-shaped source-time-functions centered at the predicted arrival times and invert the waveform data for the best fitting durations and amplitudes for each station independently to accommodate radiation patterns, path and site effects. Sub-event amplitudes and durations are assumed to be the average of the individual station amplitudes and durations, respectively. We use an iterative nonlinear least squares algorithm similar to Tsai et al. (2005) (Tsai et al., 2005) to iteratively update the sub-event locations and times by minimizing waveform misfit. The procedure requires initial guesses for sub-event model parameters, and we use our visually-determined results for both the Okhotsk and Bolivia earthquakes (plus published results for the Bolivia earthquake (Ihmlé, 1998; Kikuchi and Kanamori, 1994; Silver et al., 1995)), so that convergence is reached within 20 iterations. The choice of starting points and the number of sub-events can be adjusted based on waveform misfit and directivity analysis. Note that in this paper we assume that all sub-events occurred at the same depth. However, possibly different depths of sub-events will only bias the timing of the sub-events, but not the sub-event locations because of different azimuthal dependences.

7.4.2 Results

Figure 7.3a, 7.3b and Table 7.1a, 7.1b describe the final sub-event models for the Okhotsk and Bolivia earthquakes, respectively, where sub-event moments are assumed to be proportional to the average observed P-wave amplitudes. Waveforms are generally well fit (Figure 7.3c, 7.3d and Figure 7.4) and the sub-event models confirm the first-order features revealed by the directivity analysis. The Okhotsk earthquake first ruptured sub-event E1 slightly to the NE of the epicenter at about 8s, then proceeded to the south and ruptured its biggest sub-event E2. Perhaps due to the large slip, the rupture reset to propagate both north and south, generating E3 back near the epicenter (between E1 and E2) and E4 to the south. Finally, the rupture ended towards E4 at about 30s (see Figure 7.3a and 7.2a). The overall rupture was about 90km long, and was aligned roughly with the N-axis of the Okhotsk earthquake's GCMT focal mechanism (Ekström et al., 2012) as well as being fairly close to the slab strike from Slab 1.0 (Hayes et al., 2012) (dashed lines in Figure 7.3a) considering the uncertainties in Slab 1.0. The Bolivia earthquake started with a 10s-long weak but fast (3.5km/s) eastward rupture and generated three small sub-events (E1, E2 and E3) and a large sub-event E4 (stage 1). In stage 1, the rupture was approximately aligned with the N-axis of the Bolivia earthquake's GCMT focal mechanism (Ekström et al., 2012) and the slab strike from Slab 1.0 (Hayes et al., 2012) (dashed lines in Figure 7.3b). Similar to what happened after E2 of the Okhotsk earthquake, after E4, the Bolivia rupture also reset and changed rupture direction. However, rather than continuing along the slab strike, the rupture went to the North and NNW with E5, E6, E7, E8 and to the NE with E9. This stage is when most of the slip occurred. This main rupture area was about 30km$\times$40km, and lasted about 22s, characterizing a slow rupture speed of about 1.5km/s. In short, although the Bolivia earthquake and the Okhotsk earthquake have similar depths and moments, they have significantly different rupture processes and geometries. We find that the Okhotsk earthquake is twice as long and has rupture speed twice as high as the Bolivia earthquake. This implies that the Okhotsk earthquake has significantly lower static stress drop and higher radiation efficiency than the Bolivia earthquake. The two earthquakes' major ruptures also have different orientations with respect to the N-axes of the focal mech-

Table 7.1: Sub-event models

(a) Sub-event model of the 2013 Okhotsk earthquake

	Times (s)	Longitude (°)	Latitude (°)	Mw
I1	1.33	153.278	54.877	7.10
E1	8.94	153.347	54.898	7.95
E2	15.30	153.507	54.475	8.13
E3	22.95	153.471	54.823	7.88
E4	24.23	153.653	54.160	7.95
E4	32.27	153.656	54.135	7.42

(b) Sub-event model of the 1994 Bolivia earthquake

	Times (s)	Longitude (°)	Latitude (°)	Mw
E1	0.04	-67.561	-13.845	7.18
E2	3.34	-67.425	-13.880	7.14
E3	6.55	-67.416	-13.849	7.24
E4	11.77	-67.227	-13.884	7.71
E5	15.96	-67.208	-13.840	7.81
E6	20.67	-67.406	-13.729	7.71
E7	26.11	-67.322	-13.697	7.91
E8	35.04	-67.241	-13.764	7.51
E9	32.55	-67.003	-13.682	7.61

anisms and the local slab strikes. Additionally, both earthquakes show well-resolved dynamic rupture processes strongly affected by sub-events with large slip.

7.5 Discussion and conclusions

The new rupture models obtained here have significant implications for the mechanics of deep earthquakes. Previous studies (Tibi et al., 2003; Wiens, 2001), using sets of large deep earthquakes (M>7), have observed slow rupture velocities for events in warm subduction zones, such as the South American subduction zone, and fast rupture velocities in cold subduction zones like Tonga. Although speculative, it has been suggested that two fundamentally different faulting mechanisms might operate for deep earthquakes (Houston, 2007). For the two largest deep earthquakes studied

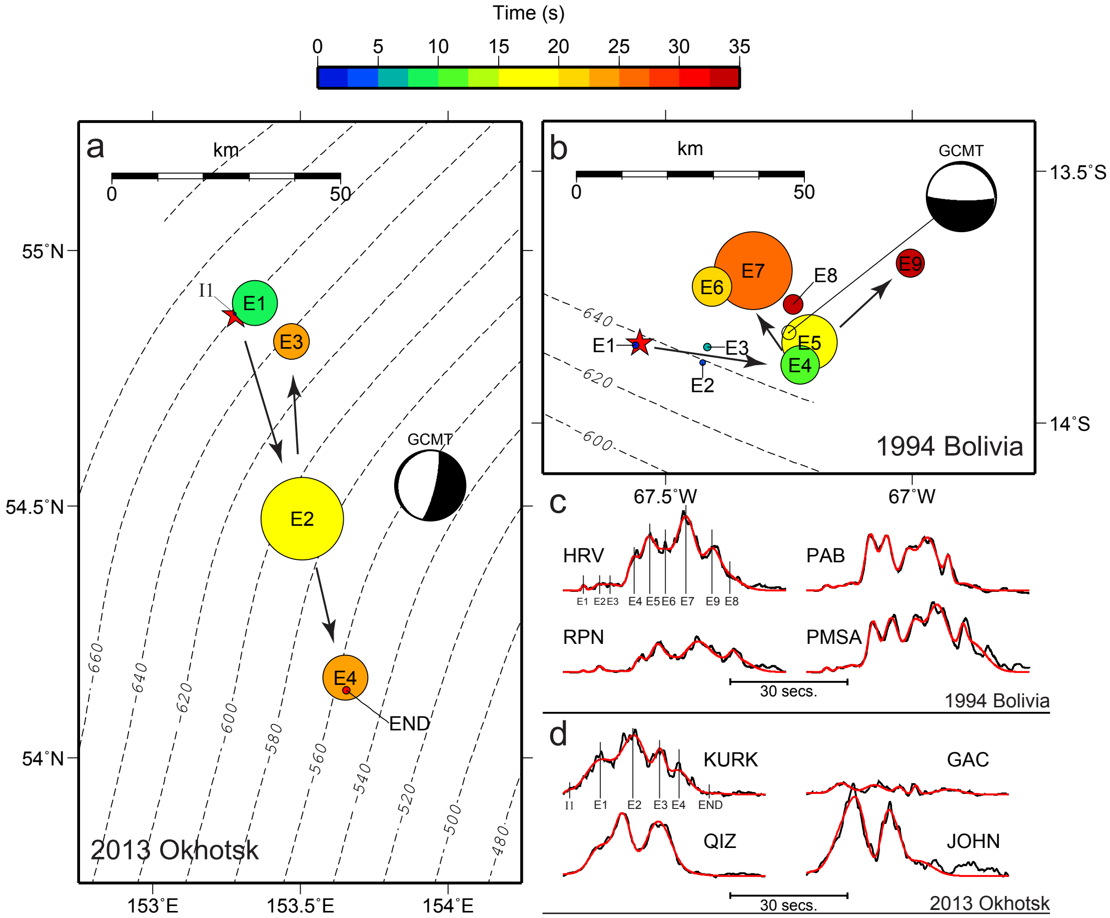

Figure 7.3: Sub-event models of the Okhotsk earthquake in (a) and of the Bolivia earthquake in (b). The red stars are the USGS NEIC epicenters, used as the reference starting points. Circles represent the earthquake sub-events with moments denoted by the sizes of the circles, and colors indicating sub-event centroid times. The black arrows illustrate the approximate rupture sequences. The slab depth contours from the Slab 1.0 model30 are shown as dashed lines. The N-axes of the Global CMT solutions of both earthquakes are approximately aligned with their respective slab strikes. (c) and (d) show example waveform fits for the sub-event models, for the Bolivia and Okhotsk earthquakes, respectively, with observed waveforms in black and predicted waveforms in red. The stations shown here are highlighted in Figure 7.1, and are representative of different azimuths. On the first example for each earthquake, the predicted arrival times of sub-events are marked by thin vertical lines. The complete waveform fits can be found in the supplementary material.

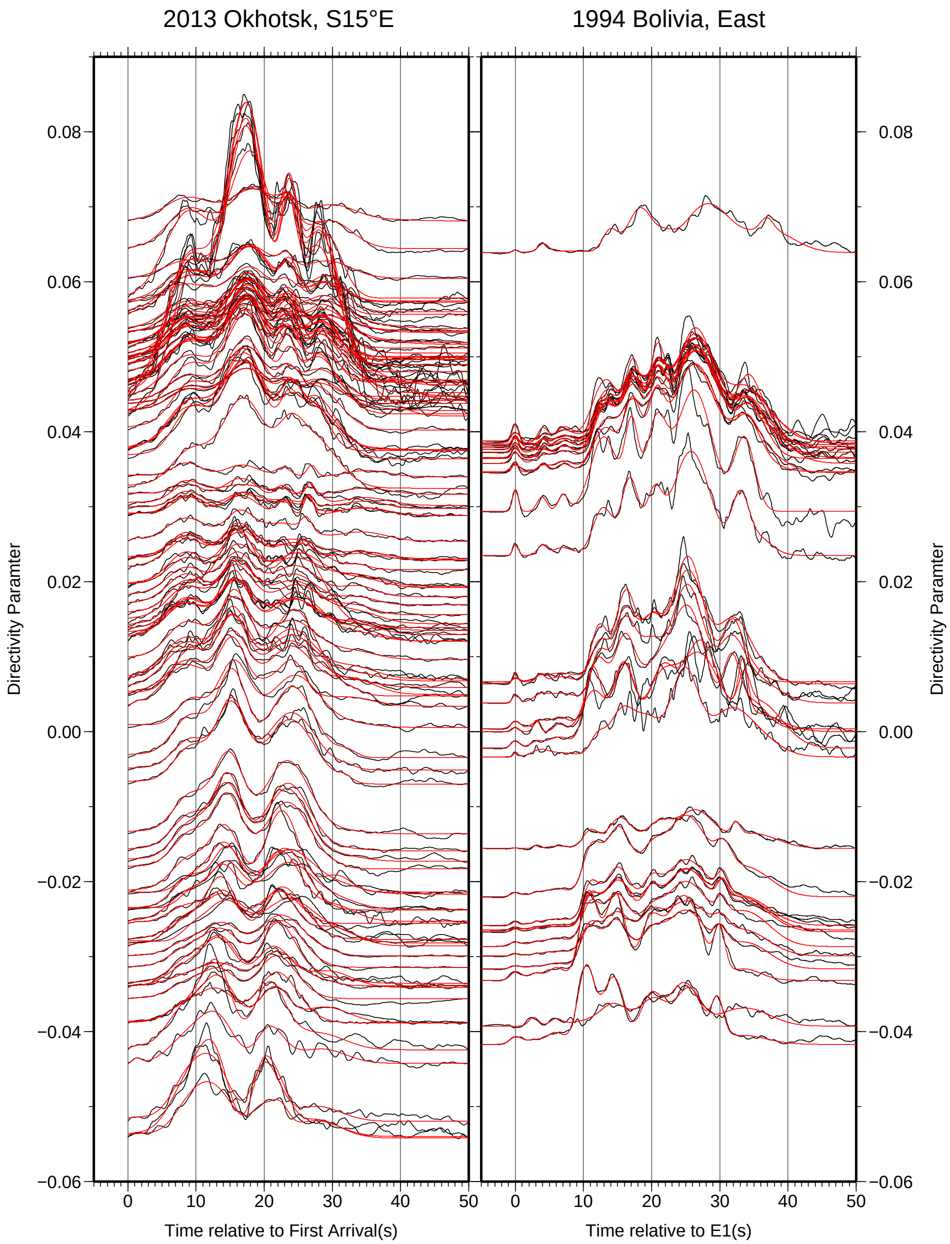

Figure 7.4: Waveform fits for the sub-event models of the 2013 Okhotsk earthquake and 1994 Bolivia earthquake. The data is plotted in black and the synthetics are plotted in red.

in this paper, the Bolivia earthquake occurred in the relatively warm South American subduction zone, whereas the Okhotsk earthquake occurred in the relatively cold Kuril subduction zone (Wiens and Gilbert, 1996). We find that they have significantly different source dimension, rupture speed, and orientation with respect to the slab strike, consistent with observations for other deep earthquakes (Tibi et al., 2003; Wiens, 2001), and resulting in different stress drops and radiation efficiencies. However, our sub-event analysis also shows that the first stage of the Bolivia earthquake, although weak, actually had a fast rupture speed, similar to the Okhotsk earthquake and other deep earthquakes in cold slabs. Furthermore, stage 1's rupture direction is also sub-parallel to the local strike of the slab, similar to the Okhotsk earthquake. From this, we infer that the Bolivia earthquake involved two different mechanisms in its two stages, with its first stage being similar to the Okhotsk earthquake except consisting of relatively small amplitude slip. Since the shear melting inferred during the Bolivia earthquake was mostly based on the major rupture parameters dominated by the area with large slip (Kanamori et al., 1998), it is reasonable to assume that the mechanism of stage 2 is shear instability caused by shear melting in a relatively warm slab.

Given our new results, we suggest a conceptual model to explain the different rupture processes of the Bolivia and Okhotsk earthquakes (Figure 7.5). Due to the difference in the thermal state of the subducting slabs responsible for the two earthquakes, the predicted widths of the metastable olivine wedges are also different. The Bolivia earthquake nucleated inside the relatively thin cold slab core by the transformational faulting mechanism (Green and Houston, 1995; Green II and Burnley, 1989; Kirby et al., 1991; Kirby et al., 1996), and ruptured inside the core along slab strike. Due to the small thickness of cold core, the rupture was relatively small but fast. However, after about 10s, the large sub-event E4 triggered shear melting, allowing the rupture to grow outside the metastable olivine wedge into the warmer slab

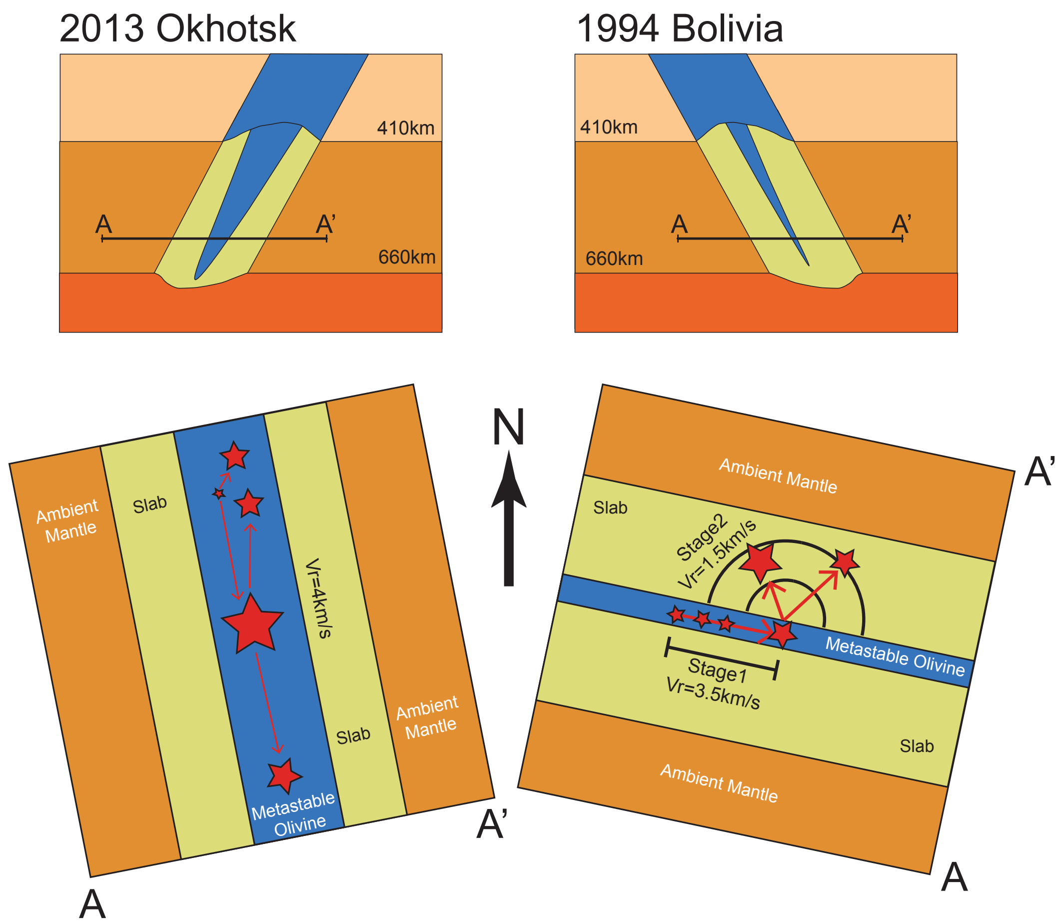

Figure 7.5: Conceptual models of the Okhotsk and Bolivia earthquakes in cross section (top panels) and map view (bottom panels). Due to differences in the thermal states of the subducting slabs in which the two earthquake occurred, the widths of the metastable olivine wedges in the slab core are also different. This causes different dominant faulting mechanisms for the two largest deep earthquakes. The Okhotsk earthquake is inferred to have ruptured mostly inside the relatively thick metastable olivine wedge, whereas the Bolivia earthquake's major rupture, stage 2, was outside the relatively thin metastable olivine wedge. See the main text for details.

material, where the melting point is reached more easily (Ogawa, 1987). The positive feedback during shear melting caused the slip to grow rapidly to cause a great earthquake. Due to the substantial energy dissipation involved with shear melting, the rupture speed in this stage decreased significantly. On the other hand, we propose that the recent Okhotsk earthquake nucleated and managed to stay inside the relatively wide metastable olivine wedge in a cold slab. Therefore, the rupture direction stayed close to the slab strike, and the rupture speed stayed relatively high. Interestingly, after the biggest sub-event E2, the rupture also seems to have reset and ruptured both northward and southward, similar to the Bolivia earthquake after its E4. This implies that very dynamic rupture processes occur during great deep earthquakes, despite inferred differences in the mechanisms. The results shown in this paper demonstrate the complexity of deep earthquakes, and the methodology described has the potential to reveal the mechanics of other earthquakes.

References

Ammon, C.J., Ji, C., Thio, H.-K., Robinson, D., Ni, S., Hjorleifsdottir, V., Kanamori, H., Lay, T., Das, S., Helmberger, D., 2005. Rupture process of the 2004 Sumatra-Andaman earthquake. Science 308, 1133-1139.

Duputel, Z., Kanamori, H., Tsai, V.C., Rivera, L., Meng, L., Ampuero, J.-P., Stock, J.M., 2012. The 2012 Sumatra great earthquake sequence. Earth and Planetary Science Letters 351, 247-257.

Ekström, G., Nettles, M., Dziewoński, A., 2012. The global CMT project 2004–2010: Centroid-moment tensors for 13,017 earthquakes. Physics of the Earth and Planetary Interiors 200-201, 1-9.

Frohlich, C., 1989. The nature of deep-focus earthquakes. Annual Review of Earth and Planetary Sciences 17, 227.

Green, H.W., Houston, H., 1995. The mechanics of deep earthquakes. Annual Review of Earth and Planetary Sciences 23, 169-214.

Green II, H., Burnley, P., 1989. A new self-organizing mechanism for deep-focus earthquakes. Nature 341, 733-737.

Griggs, D., Baker, D., 1969. The origin of deep-focus earthquakes, in: Mark, H., Fernbach, S. (Eds.), Properties of Matter Under Unusual Conditions. Wiley, New York, pp. 23-42.

Hayes, G.P., Wald, D.J., Johnson, R.L., 2012. Slab1. 0: A three-dimensional model of global subduction zone geometries. Journal of Geophysical Research 117, B01302.

Houston, H., 2007. Deep earthquakes. Treatise on Geophysics, edited by G. Schubert, 321-350.

Ihmlé, P.F., 1998. On the interpretation of subevents in teleseismic waveforms: the 1994 Bolivia deep earthquake revisited. Journal of Geophysical Research 103, 17919-17932.

Ishii, M., Shearer, P.M., Houston, H., Vidale, J.E., 2005. Extent, duration and speed of the 2004 Sumatra–Andaman earthquake imaged by the Hi-Net array. Nature 435, 933-936.

Kanamori, H., Anderson, D.L., Heaton, T.H., 1998. Frictional melting during the rupture of the 1994 Bolivian earthquake. Science 279, 839-842.

Karato, S.-i., Riedel, M.R., Yuen, D.A., 2001. Rheological structure and deformation of subducted slabs in the mantle transition zone: implications for mantle circulation and deep earthquakes. Physics of the Earth and Planetary Interiors 127, 83-108.

Kikuchi, M., Kanamori, H., 1991. Inversion of complex body waves—III. Bulletin of the Seismological Society of America 81, 2335-2350.

Kikuchi, M., Kanamori, H., 1994. The mechanism of the deep Bolivia earthquake of June 9, 1994. Geophysical Research Letters 21, 2341-2344.

Kirby, S.H., Durham, W.B., Stern, L.A., 1991. Mantle Phase Changes and Deep-Earthquake Faulting in Subducting Lithosphere. Science 252, 216-225.

Kirby, S.H., Okal, E.A., Engdahl, E.R., 1995. The 9 June 94 Bolivian deep earthquake: An exceptional event in an extraordinary subduction zone. Geophysical Research Letters 22, 2233-2236.

Kirby, S.H., Stein, S., Okal, E.A., Rubie, D.C., 1996. Metastable mantle phase transformations and deep earthquakes in subducting oceanic lithosphere. Reviews of Geophysics 34, 261-306.

Meade, C., Jeanloz, R., 1991. Deep-focus earthquakes and recycling of water into the Earth's mantle. Science 252, 68-72.

Ogawa, M., 1987. Shear instability in a viscoelastic material as the cause of deep focus earthquakes. Journal of Geophysical Research 92, 13801-13810.

Persh, S.E., Houston, H., 2004a. Deep earthquake rupture histories determined by global stacking of broadband P waveforms. Journal of Geophysical Research 109, B04311.

Persh, S.E., Houston, H., 2004b. Strongly depth-dependent aftershock production in deep earthquakes. Bulletin of the Seismological Society of America 94, 1808-1816.

Silver, P.G., Beck, S.L., Wallace, T.C., Meade, C., Myers, S.C., James, D.E., Kuehnel, R., 1995. Rupture characteristics of the deep Bolivian earthquake of 9 June 1994 and the mechanism of deep-focus earthquakes. Science 268, 69-69.

Suzuki, M., Yagi, Y., 2011. Depth dependence of rupture velocity in deep earthquakes. Geophysical Research Letters 38, L05308.

Tibi, R., Bock, G., Wiens, D.A., 2003. Source characteristics of large deep earthquakes: Constraint on the faulting mechanism at great depths. Journal of Geophysical Research 108, 2091.

Tocheport, A., Rivera, L., Chevrot, S., 2007. A systematic study of source time functions and moment tensors of intermediate and deep earthquakes. Journal of Geophysical Research 112, B07311.

Tsai, V.C., Nettles, M., Ekström, G., Dziewonski, A.M., 2005. Multiple CMT source analysis of the 2004 Sumatra earthquake. Geophysical Research Letters 32, L17304.

Wiens, D.A., 2001. Seismological constraints on the mechanism of deep earthquakes: Temperature dependence of deep earthquake source properties. Physics of the Earth and Planetary Interiors 127, 145-163.

Wiens, D.A., Gilbert, H.J., 1996. Effect of slab temperature on deep-earthquake aftershock productivity and magnitude-frequency relations. Nature 384, 153-156.

Wiens, D.A., McGuire, J.J., 1995. The 1994 Bolivia and Tonga events: Fundamentally different types of deep earthquakes? Geophysical Research Letters 22, 2245-2248.